Surface Photovoltage Study of Metal Halide Perovskites Deposited Directly on Crystalline Silicon

Vesselin Donchev, Davide Regaldo, Stefan Georgiev, Aleksandra Bojar, Mattia da Lisca, Kiril Kirilov, J Alvarez, Philip Schulz, Jean-Paul Kleider

ACS OMEGA

http://pubs.acs.org/journal/acsodf

Perspective

Surface Photovoltage Study of Metal Halide Perovskites Deposited Directly on Crystalline Silicon

Vesselin Donchev,* Davide Regaldo, Stefan Georgiev, Aleksandra Bojar, Mattia da Lisca, Kiril Kirilov, José Alvarez, Philip Schulz, and Jean-Paul Kleider

Cite This: *ACS Omega* 2023, 8, 8125−8133

Read Online

ACCESS | Metrics & More | Article Recommendations | Supporting Information

ABSTRACT: Perovskite (PVK) films deposited directly on n-type crystalline Si substrates were investigated by two operating modes of the surface photovoltage (SPV) method: (i) the metal−insulator−semiconductor (MIS) mode and (ii) the Kelvin probe force microscopy (KPFM). By scanning from 900 to 600 nm in the MIS mode, we consecutively studied the relatively fast processes of carrier generation, transport, and recombination first in Si, then on both sides of the PVK/Si interface, and finally in the PVK layer and its surface. The PVK optical absorption edge was observed in the range of 1.61−1.65 eV in good agreement with the band gap of 1.63 eV found from photoluminescence spectra. Both SPV methods evidenced an upward energy band bending at the PVK/n-Si interface generating positive SPV. Drift−diffusion modeling allowed us to analyze the shape of the wavelength dependence of the SPV. It was also observed that the intense illumination in the KPFM measurements induces slow SPV transients which were explained by the creation and migration of negative ions and their trapping at the PVK surface. Finally, aging effects were studied by measuring again SPV spectra after one-year storage in air, and an increase in the concentration of shallow defect states at the PVK/n-Si interface was found.

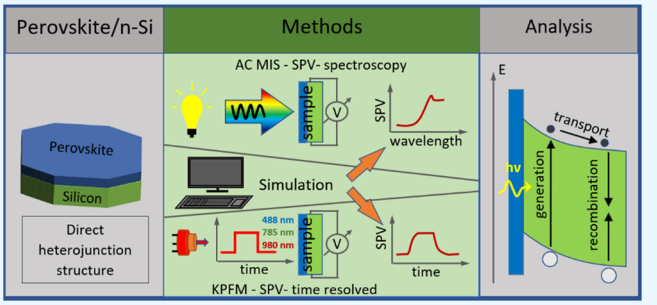

1. INTRODUCTION

The noticeable success of halide perovskites (PVKs) in the field of photovoltaics has generated many investigations of their optoelectronic properties by various experimental techniques. In particular, the surface photovoltage (SPV) method has been widely used to study and optimize materials and junctions composed of halide perovskite absorbers regarding the presence of intraband gap states, which are harmful to the performance of these materials in devices. For example, SPV spectroscopy has been used by Levine et al.[1] to evidence the existence of deep defects that can act as efficient recombination centers and enhance trap-assisted recombination in mixed-cation lead tribromide $(FA_{0.85}MA_{0.1}Cs_{0.05})$-$PbBr_3$ perovskites. Zu et al.[2] have demonstrated a downward bending of the conduction and valence bands at the PVK surface, which was attributed to the presence of donor-type surface states, likely due to elemental lead. Ma et al.[3] have shown that increasing temperature leads to a decrease in the surface band bending, which, together with the enhanced lattice vibration scattering, decreases the SPV. The different behavior of this effect occurring in the grains and at the grain boundaries has led them to the conclusion about a phase transition from the tetragonal phase to the cubic phase at around 50 °C. A similar phase transition was observed by Dittrich et al.[4] together with a decrease of the band gap with decreasing temperature. Futscher and Deibel[5] have emphasized that metal halide perovskites are mixed ionic−electronic conductors and one needs to be careful whether the measured signals are due to ionic or electronic defects. The activation energies for ion migration decrease upon light illumination.[6] Armaroli et al.[7] have investigated the changes in the SPV of methylammonium lead tribromide PVK single crystals upon X-ray excitation. They observed the formation of bromine vacancies which influence the coupling between photogenerated carriers and optical lattice phonons, creating large polarons. Levine et al.[8] have discussed how to avoid possible artefacts in SPV spectroscopy measurements of perovskites.

Despite these works employing the SPV technique, the interpretation of the SPV data on perovskites is still questionable and needs further experimental studies as well as appropriate analysis with the help of a proper simulation of the experiment. In particular, extensive work is carried out to achieve a better understanding of carrier generation, transport, and recombination in perovskite−silicon tandems. Such tandem solar cells have received considerable research interest

Received: November 30, 2022
Accepted: February 17, 2023
Published: February 24, 2023

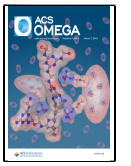

and development in the last few years since they are a prospective system for overcoming the single-cell efficiency limit.[9] This is due to the matured Si technology combined with the well-suited optoelectronic properties of the perovskite materials such as a tunable band gap around 1.6 eV via compositional engineering, high absorption coefficient, and steep absorption edge.[10,11] Already much research is ongoing on two-terminal and four-terminal PVK/Si tandem solar cells,[9,12−15] where these two materials are not in direct contact and such tandems are currently showing efficiencies as high as 31.3%.[16] Recently, Mariotti et al. have demonstrated that it is possible to create a photovoltaic device based on the direct heterojunction between PVK and n-Si.[17] However, further research is needed to fully understand and exploit the PVK/Si system with direct contact between the two materials. Knowledge of the carrier transport and band alignment at the PVK/Si interface would allow for a better understanding of their compatibility and attainable performance levels. However, research on such PVK/Si direct heterojunction structures is still rarely conducted.

Preliminary results from surface photovoltage methods on PVK films deposited directly onto crystalline silicon (c-Si) wafers have been recently obtained.[18] Here, we focus on structures on n-type c-Si and we develop a thorough analysis of the SPV spectroscopy, i.e., the spectral dependence of SPV, with the support from numerical modeling to get more insight into carrier generation, transport, and recombination in this system. In addition, we present the results of measurements performed both after the preparation of the samples and one year later to examine ageing effects.

2. EXPERIMENTAL SECTION

Triple cation mixed halide PVK thin films were deposited via spin-coating directly on n-type c-Si substrates. The PVK composition was $Cs_{0.05}(MA_{0.14},FA_{0.86})_{0.95}Pb(I_{0.84},Br_{0.16})_3$, where MA is methylammonium and FA is formamidinium. Details concerning the source materials used and the applied procedure can be found in ref 18. Scanning electron microscopy images evidenced a high-quality surface of the PVK layers, which fully and quite homogeneously covered the Si substrates. The film thickness was between 400 and 500 nm. X-ray diffraction measurements revealed the highly crystalline nature of the PVK films exhibiting the dominant PVK phase and small amounts of a foreign phase originating from PbI_2.[18]

Two different operating modes of the SPV method were applied to characterize the samples: (i) the metal−insulator−semiconductor (MIS) operation mode using chopped light with low intensity[19] and (ii) the Kelvin probe force microscopy (KPFM) with continuous illumination at higher intensity.[20] These two techniques can capture the processes of carrier generation, transport, and recombination at different time scales: slow processes are revealed by KPFM where the SPV can be recorded over a long time, while the AC SPV-MIS mode can reveal faster processes. Thus, the two techniques are complementary allowing the acquisition of a more complete picture of the processes occurring in the sample under illumination with different wavelengths and at different time scales.

The SPV-MIS spectra were recorded at room temperature with the setup described in ref 21. The probe electrode was a semitransparent SnO_2 film evaporated on the bottom surface of quartz glass. The sample was positioned on a grounded copper platform and separated from the probe electrode by a 15 μm thick mica sheet (Figure 1). The excitation used a 250 W halogen lamp along with a SPEX grating monochromator (f = 0.25 m), filters to cut off higher-order diffraction, and an optical chopper tuned at 94 Hz. The scanning was performed from long toward short wavelengths (λ) in the spectral range from 900 to 600 nm keeping the photon flux density value constant around 10^{13} cm^{-2} s^{-1}. For that purpose, part of the light was deflected toward an Oriel IR50 Golay detector (which has a flat spectrum) connected to a lock-in amplifier (Brookdeal 9530). This feedback was used to adjust the position of a neutral density filter with graded optical density, thus achieving control of the photon flux density with an accuracy of ∼1%. The probe signal relative to the ground was fed to a high-impedance unity gain buffer and then measured by a lock-in amplifier (SR830). To study the SPV phase delay relative to the light excitation in a correct way, we considered and eliminated the possible phase shifts between (i) the SPV and the voltage measured by the lock-in amplifier and (ii) the light modulation and the reference signal generated by the optical chopper, following the procedures described in ref 21.

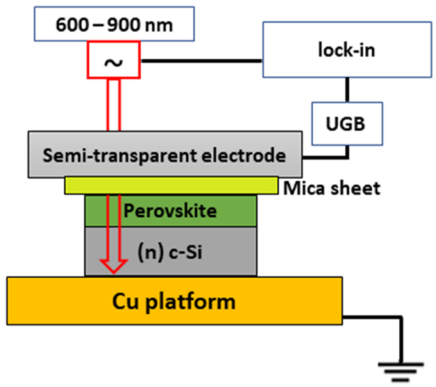

Figure 1. Schematic of the PVK/(n) c-Si sample arrangement in the SPV-MIS setup. UGB denotes the unity gain buffer used for impedance matching.

KPFM measurements were performed in ambient conditions by a HORIBA/AIST-NT (TRIOS platform) scanning probe microscopy system using a conductive Pt/Ir AFM tip. For detection of the cantilever deflection, a laser diode emitting at 1310 nm is used, thus avoiding unwanted band-to-band light excitation of any of the sample components.[18] The contact potential difference (CPD) between the tip and the sample was measured scanning over an area of 2 × 2 μm^2 and the results were averaged for each horizontal line. CPD transients were recorded over time scales of minutes after switching on and off the illumination from three laser diodes with wavelengths of 980, 785, and 488 nm, respectively, and a photon flux density of approximately 5 × 10^{17} cm^{-2} s^{-1}. The SPV was then obtained by subtracting the CPD measured in the dark from the one measured under illumination.[18] A schematic of the sample during SPV measurements with the KPFM setup is shown in Figure 2.

The KPFM measurements were performed shortly after the samples were prepared, while two sets of SPV-MIS measurements were carried out. The first set was completed one month after the KPFM measurements, meantime keeping the samples in a dark box with desiccant. The second set was carried out one year later, keeping the samples in a dark box in air between the two sets.

https://doi.org/10.1021/acsomega.2c07664
ACS Omega 2023, 8, 8125−8133

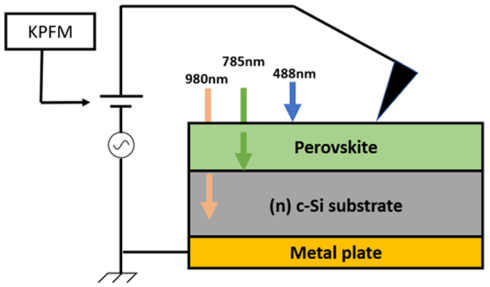

Figure 2. Schematic of the PVK/n-Si sample during SPV measurements in the KPFM setup.

3. SPV MEASUREMENTS IN THE MIS MODE

The SPV amplitude spectrum is known to emulate the optical absorption spectrum, while the SPV phase indicates the direction of the photocarrier transport in the sample.[19,21] The interpretation of the SPV amplitude and phase spectra is easier when the vector model of the SPV signal is applied.[22]

Figures 3 and 4 display the spectra of the SPV-MIS amplitude and phase, respectively, recorded in a PVK/(n) c-Si

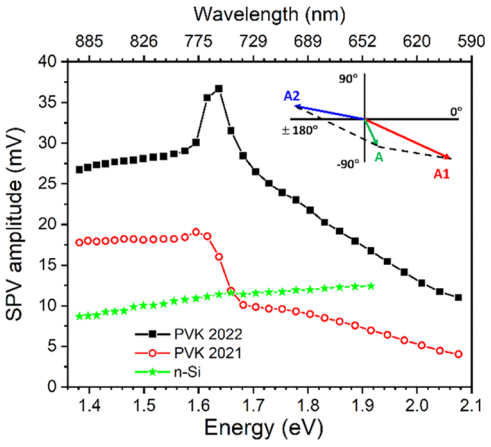

Figure 3. SPV amplitude spectra of a PVK/(n) c-Si structure measured after one-month storage in a box with desiccant (measurement set 1 labeled PVK 2021, circles) and after storage for one year in the dark in ambient conditions (measurement set 2 labeled PVK 2022, squares). The SPV amplitude of a bare Si substrate is shown with stars. The vector diagram in the inset shows the interplay of the SPV components from the interface (A1) and the PVK surface (A2) resulting in the overall measured SPV signal (A).

sample in the range of 1.38−2.08 eV (900−600 nm) after one-month storage in a box with desiccant (measurement set 1 labeled PVK 2021) and after storage for one year in the dark in ambient conditions (measurement set 2 labeled PVK 2022).

First, we discuss the spectra from measurement set 1. For photon energies $h\nu$ in the range of 1.38−1.55 eV (800 nm < λ < 900 nm), the PVK layer is transparent and light is fully absorbed in the silicon. The signal in this range is strong indicating a significant space charge region (SCR) at the PVK/n-Si interface. The phase values in the IVth quadrant (between 0 and −90°, Figure 4) show that photogenerated electrons predominantly move toward the bulk, while holes move toward the surface, which results in positive SPV.[21] Therefore, the energy band bending is upward in the direction toward the surface. When increasing $h\nu$ slightly above 1.55 eV (λ < 800 nm), a slight increase of the amplitude is observed, which is

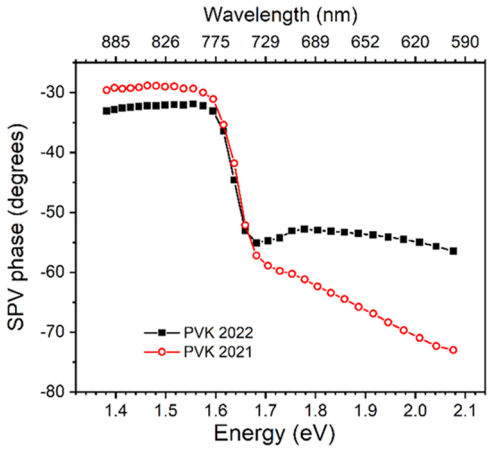

Figure 4. SPV phase spectra of the same PVK/(n) c-Si structure as in Figure 3, measured after one-month storage in a box with desiccant (measurement set 1 labeled PVK 2021, circles) and after storage for one year in the dark in ambient conditions (measurement set 2 labeled PVK 2022, squares).

better manifested in the spectrum measured one year later (see below). However, on further increasing $h\nu$ above 1.61 eV (λ < 770 nm), the amplitude rapidly drops and continues decreasing up to 2.08 eV revealing a shoulder in the range of 1.67−2.08 eV. This is accompanied by an increase of the SPV phase delay relative to the excitation (a decrease of the SPV phase values in the IVth quadrant). It is interesting to note that quite similar spectral features were observed in the external quantum efficiency (EQE) spectra of several PVK/n-Si heterojunction structures as reported by Mariotti et al.[17] Because of the sharp cutoff in the photoresponse for photon energies above the PVK band gap energy, these authors concluded that the PVK/n-Si junction is one-sided and the SCR lies in the silicon, while the PVK acts as a "parasitic absorber".[17] Assuming such interpretation, the PVK band gap can be assessed to be in the range of 1.61−1.65 eV (770 −750 nm) which corresponds to the sharp cutoff of the SPV amplitude. This is in good agreement with the band gap of 1.63 eV (760 nm) found from PL measurements.[18]

For $h\nu$ above the PVK band gap, the absorption in the silicon is strongly reduced and practically disappears with further increasing $h\nu$. The SPV signal is however not zero, similar to the EQE spectrum from ref 17. We consider two components of the SPV signal in this range. The first component is due to photocarriers generated in the PVK that reach the PVK/n-Si interface by diffusion where they are separated by the built-in electric field to give rise to an SPV signal with phase in the IVth quadrant (positive SPV). With further increasing $h\nu$, the absorption is more and more concentrated near the PVK surface. KPFM transients under 488 nm (2.54 eV) excitation have shown a downward energy band bending at the surface[18] (see also below), which agree with other reports.[2] The downward band bending induces a second component of the SPV signal with a phase in the IInd quadrant (negative SPV, phase between 90 and 180°).[21] Its magnitude increases with increasing $h\nu$. The interaction of the two SPV components with nearly opposite phases can explain the decrease of both SPV amplitude and phase observed for $h\nu$ above 1.65 eV. This idea can be better understood from the vector diagram shown in the inset of Figure 3, where vector A1 (A2) corresponds to the SPV component from the interface

https://doi.org/10.1021/acsomega.2c07664
ACS Omega 2023, 8, 8125−8133

(surface), while A represents the overall measured SPV signal. With increasing $h\nu$, vector A2 increases, while vector A1 decreases. As a result, vector A rotates clockwise and decreases in magnitude in line with the observations in Figure 3. The overall SPV remains in the IVth quadrant, which shows that the interface component is stronger than the surface component. This may be explained by the small PVK layer thickness easing carrier diffusion and the strong built-in field in the SCR at the interface.

Looking at the SPV amplitude spectrum from measurement set 2 (Figure 3, squares), the increase of the amplitude in the spectral range immediately below the PVK band gap energy (1.57−1.63 eV) is better manifested as compared to measurement set 1. We have checked that the SPV amplitude of the bare n-Si substrate changes nearly linearly in the range of 1.38−1.91 eV (900−650 nm), as shown in Figure 3 (star symbols). Therefore, the step-like increase observed in the range of 1.57−1.63 eV (790−760 nm) in Figure 3 is related to the presence of the PVK. It is tentatively ascribed to the inclusion of below-band-gap optical transitions with the participation of shallow defect levels and one of the bands in the PVK at its interface with n-Si. At room temperature, the shallow levels release the photogenerated carriers, which are separated by the interface's built-in electric field to give rise to the SPV. The increase of this feature in the spectrum measured after storage of the sample for one year in the dark in ambient conditions suggests an increase in the density of defect states in the PVK due to aging processes. Generation of SPV via such transitions should be a slower process as compared to band-to-band transitions. Therefore, it will be affected by the light chopping frequency (see below). At energies above 1.64 eV, the amplitude spectrum is similar to the one from measurement set 1 revealing the sharp cutoff at the PVK band gap and a continuous decrease for increasing energy. The combination of two SPV components with nearly opposite phases again explains the spectral shape. The SPV phase decreases less than the phase in measurement set 1 (see Figure 4). In terms of the vector diagram from Figure 3, this may indicate a relatively stronger contribution from the PVK/n-Si interface as compared to the PVK surface in this case.

Figure 5 compares two SPV spectra from the second set of measurements recorded at 94 and 492 Hz. As usual, at higher frequencies the SPV amplitude decreases and the SPV phase delay relative to the excitation increases.[21] However, another effect induced by the high frequency is the strong reduction of amplitude step in the range of 1.57−1.63 eV. This finding supports the idea presented above that the increase of the SPV amplitude in the range of 1.57−1.63 eV observed at low frequency is due to defect-related optical transitions at the PVK/n-Si interface, which are slower as compared to band-to-band transitions.

4. SPV MEASUREMENTS IN THE KPFM MODE

Figure 6 displays the SPV transients measured by KPFM in a PVK/(n) c-Si sample after switching on and off the illumination using one of the three laser diodes with wavelengths of 980, 785, and 488 nm, respectively. The illumination with these three different wavelengths probes different regions of the sample. The excitation of the sample, in this case, is more than four orders of magnitude higher as compared to the SPV-MIS measurements. Therefore, effects related to the creation of ions and their migration can be

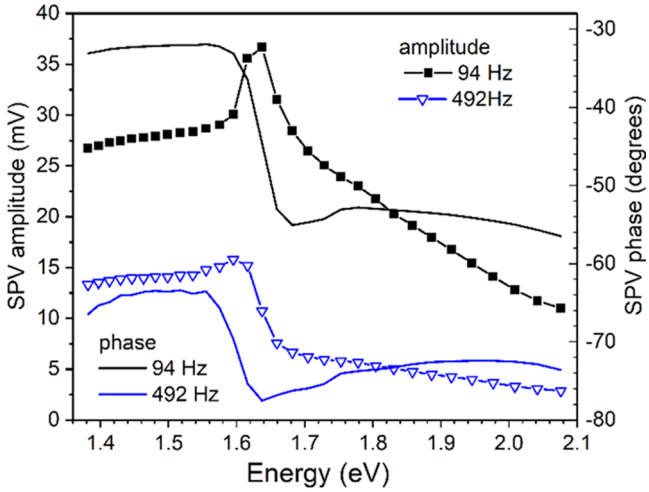

Figure 5. SPV amplitude (symbols) and phase (lines) spectra of the same PVK/(n) c-Si structure as in Figures 3 and 4, measured after storage for one year in the dark in ambient conditions (measurement set 2) at 94 Hz (black) and 492 Hz (blue).

expected having in mind that the ion activation energies decrease upon illumination levels of this order of magnitude.[6]

The light with a wavelength of 980 nm is absorbed only in the silicon. In agreement with the SPV-MIS results, one observes a high positive SPV signal (Figure 6a) due to electron−hole separation in the silicon SCR at the interface. A small decrease of the positive SPV occurs within the first 1−2 min followed by constant values for the remaining time of illumination. After the light is turned off, the signal changes polarity and a negative transient develops toward zero volt lasting around 2.5 min.

The slow SPV behavior may have different origins. One possibility is the effect of interface states that can trap some charges under illumination and slowly release them in the dark. The decrease of the signal under illumination and the negative transient after the light is turned off suggest that these charges are predominantly negative. Accumulated at the interface, they decrease the potential (increase the electron energy), thus creating negative SPV, which slowly disappears in the dark together with their number.

On the other hand, the activation energies for the migration of iodine ions in halide perovskites have been reported to be around 0.6 eV or below and decrease upon a relatively high level of illumination.[6,23] Slow reversible processes occurring upon above-band-gap illumination have been reported in halide PVKs and explained by the migration of negative ions.[24] We are not aware of studies reporting similar processes for sub-band-gap illumination. However, the relatively slow transients observed in Figure 6a suggest the existence of long-term processes occurring under 980 nm illumination and after the light is switched off. The processes induced by sub-band-gap illumination in halide PVKs are still not completely clarified and require further studies. Nevertheless, if we assume the creation of negative ions upon sub-band-gap illumination followed by ion migration, we could explain the slow transients in Figure 6a as follows: The negative ions can drift in the surface built-in electric field (downward energy band bending) and accumulate at the PVK surface until a dynamic equilibrium between drift and back diffusion establishes. This will produce a negative SPV component, which will saturate with time. In the dark, the electron and holes recombine and the positive

https://doi.org/10.1021/acsomega.2c07664
ACS Omega 2023, 8, 8125−8133

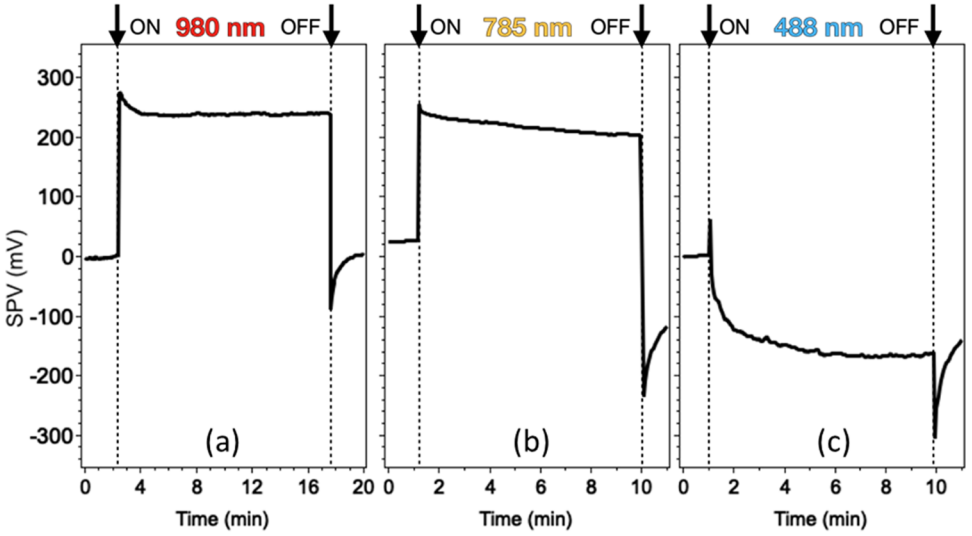

Figure 6. SPV transients measured by KPFM in a sample PVK/(n) c-Si after switching on and off the illumination of three laser diodes with wavelengths 980 nm (a), 785 nm (b), and 488 nm (c). The moments of switching on and off the light are indicated. (Adapted with permission from "Surface photovoltage characterization of metal halide perovskite on crystalline silicon using Kelvin probe force microscopy and metal–insulator–semiconductor configuration", Aleksandra Bojar, Davide Regaldo, José Alvarez, David Alamarguy, Vesselin Donchev, Stefan Georgiev, Philip Schulz and Jean-Paul Kleider; EPJ Photovolt., 13 (2022) 18, DOI: 10.1051/epjpv/2022016. Copyright CC BY 4.0, 2022, EDP Sciences).

SPV component from the interface quickly disappears. The slow release of the ions from the surface toward the bulk will account for the negative SPV transient observed in Figure 6a.

According to the PVK absorption spectrum,[18] the light with a wavelength of 785 nm is partially absorbed in the PVK but a major part of it still reaches the silicon. In this case, we consider that the interface component of the SPV signal includes electrons and holes photogenerated in the silicon, as well as electrons and holes photogenerated in the PVK, which diffuse toward the interface and get separated in the SCR of the silicon. The surface component includes electron–hole separation in the surface built-in electric field resulting in a negative SPV. Under illumination, one observes a strong positive signal, which shows that the interface component is stronger. The signal slowly decreases with time. This may be related to the slow drift of negative ions in the built-in electric field toward the PVK surface as explained above, resulting in a second negative SPV component, which slowly increases with time. The interplay of the positive and negative SPV components leads to the observed time behavior.

When the light is turned off, a negative peak occurs, followed by an SPV transient toward zero. The peak is deeper and the relaxation kinetics is much slower as compared to the case of 980 nm (the steady state is not reached for the time presented in Figure 6b). This is explained by a larger concentration of negative ions accumulated at the PVK surface during illumination, due to the larger photon energy used for excitation in this case. The negative ions slowly leave the surface when the light is turned off, which leads to the observed transient.

We have calculated that at 488 nm illumination, the absorption is concentrated in a narrow region near the PVK surface of less than 50 nm. The negative SPV under illumination in Figure 6c shows that the surface SPV component dominates. This may be explained by the lack of carrier generation in the silicon, strong carrier generation within a thin region near the PVK surface, as well as increased activation of negative ions which drift to the surface. The component from the interface includes electrons and holes photogenerated in the PVK, which diffuse toward the interface. It can account for the short positive peak appearing immediately when the light is switched on (Figure 6c). Its effect is however quickly overpowered by the negative SPV component. The negative SPV signal increases in absolute values revealing a fast and a slow component. We attribute the fast component to electron–hole separation in the surface SCR, while the slow process can be ascribed to the creation and movement toward the surface of negative ions.[25,26] When the light is turned off, the SPV components resulting from electrons and holes movement rapidly vanish with the carrier recombination. However, the negative ions accumulated at the surface remain for a long time causing even stronger negative SPV values revealed as a deep negative peak which disappears very slowly.

The long-term effects with characteristic times of seconds to minutes observed in the KPFM transients and attributed to ion migration or PVK surface decomposition are not seen in our SPV-MIS experiments. One of the reasons is the chopped light (94 Hz) used which probes faster processes over time scales of the order of 0.01s. Another reason is that the excitation, in this case, is less likely to cause noticeable creation and movement of ions because its intensity is several orders of magnitude lower compared to the light from the laser diodes used in KPFM. This explains the differences in the SPV results obtained by the two techniques, especially at high photon energies.

5. SIMULATION OF THE SPV SPECTRA

To propose an explanation for the presented SPV spectra (SPS), which show a significant drop of the SPV amplitude for photon energies above the PVK band gap, we have employed drift–diffusion simulations using the ATLAS commercial code from Silvaco Inc.

We concentrated on keeping our model as simple as possible, to minimize the degrees of freedom of the simulation. All of the model parameters are listed in Table S1. We have

https://doi.org/10.1021/acsomega.2c07664
ACS Omega 2023, 8, 8125–8133

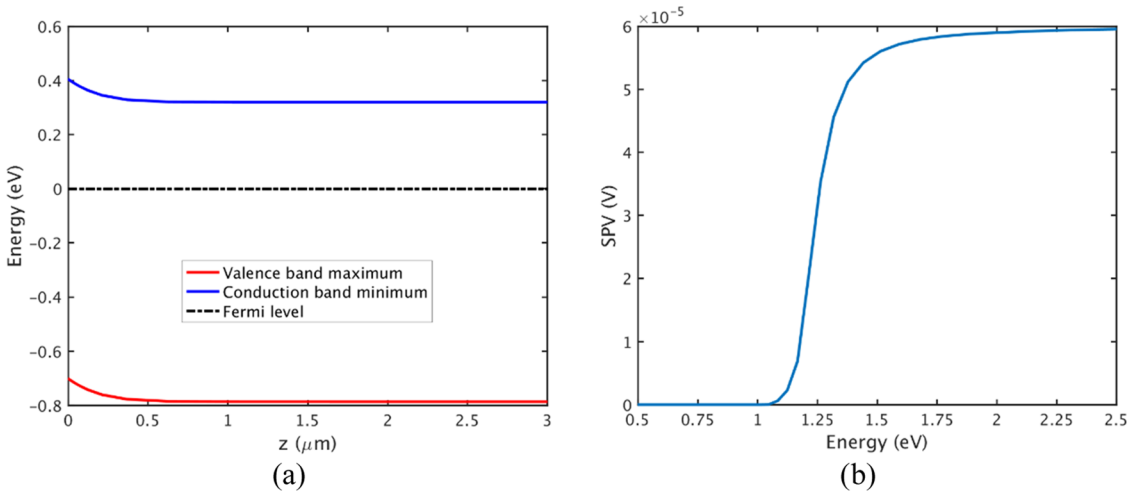

Figure 7. Band diagram (a) and SPS curve (b) obtained from drift−diffusion simulations of an n-type c-Si wafer with surface electronic traps (see text).

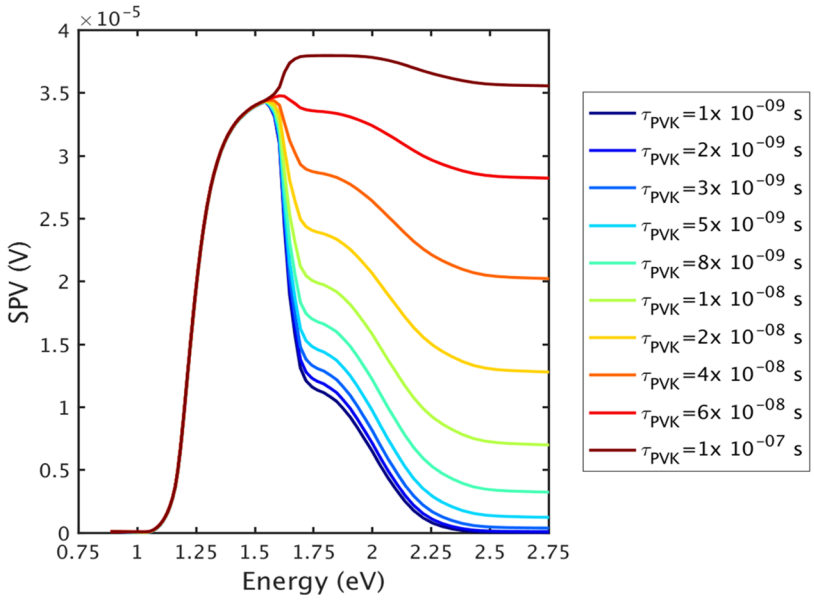

Figure 8. SPS curves obtained from drift−diffusion simulations of the PVK/Si stack, varying the nonradiative bulk lifetime (τ_{PVK}) of the PVK.

modeled the time-dependent SPV of bare n-type silicon (250 μm thick) under chopped light illumination, whose wavelength was varied to match the experimental range. At the silicon surface, and down to 1 nm depth, we placed a layer of electronic traps, namely, acceptors and donors, located respectively at 0.28 and 0.26 eV from the corresponding band edge (conduction or valence, respectively). This is carried out to recreate the defective silicon surface, which possesses amphoteric traps.[27] To realize equilibrium, these traps exchange carriers with the bulk silicon layer, creating a surface SCR (Figure 7a). Under illumination, carriers generated close to the SCR are separated by the associated electric field and therefore generate an SPV. The response of n-Si is an S-shape SPS which is centered close to the silicon band gap (Figure 7b).

To simulate the SPS for PVKs on silicon, we proceeded by adding a higher band gap undoped semiconductor on top of the silicon. This material possesses low carrier mobilities (μ_e = μ_h = 1.5 cm^2/Vs), which are typical for PVK thin films.[28] The absorption coefficient applied to this semiconductor derives from measurements of the perovskite material performed in our laboratories, and it is shown in Figure S1. We added Shockley−Read−Hall nonradiative recombination in the simulated material, which takes into account carrier losses due to defects, and reduces the steady-state carrier density under illumination. This assumption is common in the literature, and it is usually supported by quasi-Fermi level splitting (QFLS) measurements. The QFLS extrapolated from photoluminescence measurements on both complete and incomplete perovskite solar cells is always considerably lower than the QFLS reachable in the radiative limit.[29,30] This implies the presence of nonradiative recombination centers deep in the band gap in non-negligible amounts.

The added nonradiative pathway is characterized by a lifetime, and it does not consider defect charging and discharging. Considering the mobility reported above, and the Einstein relation, if we vary this lifetime between 10^{-9} and 10^{-7} s, we obtain a carrier diffusion length which ranges between 62.4 and 624 nm. Crucially, the PVK thickness falls inside this window (h_{PVK} = 450 nm).

https://doi.org/10.1021/acsomega.2c07664
ACS Omega 2023, 8, 8125−8133

The SPS of the PVK/Si structure is presented in Figure 8 for several values of the nonradiative bulk lifetime (τ_{PVK}) of the PVK. In the range 0.88−1.63 eV, it follows the SPS of Si. As the only absorbing material in this range is silicon, the PVK does not have an active role in the SPV formation in the model. When the incoming photon energy overcomes the PVK band gap, carriers start to be generated inside the PVK. Due to its large absorption coefficient (see Figure S1), most of the incoming photons are absorbed in the PVK.

For the upper end of the lifetime range reported above, the majority of the photogenerated carriers in the PVK can reach the interface: the SPV is enhanced. While carrier generation in silicon spreads far from the interface for photon energy around 1.55 eV so that not all of them contribute to the SPV, for energies slightly larger than the PVK band gap more carriers are generated closer to the interface and can be injected into the silicon layer where they can be separated by the SCR electric field.

For the lower end of the aforementioned lifetime range, the photogenerated carriers in the PVK are mostly unable to reach the interface, and therefore, as the incoming wavelength decreases and the carriers photogenerated close to the surface, the SPV decreases. The shoulder present in the SPS at around 1.77 eV (700 nm) is a direct effect of the features of the PVK absorption coefficient (Figure S1). It is in good agreement with the experimental SPV amplitude spectrum (Figure 3). Note that the SPV obtained here is much smaller than experimentally observed. In the Supporting Material, we show that with equal defect concentrations but energy positions closer to midgap the calculated SPV can be strongly increased and be in the millivolt range similar to the experimental results. This may indicate that the defect distribution at the silicon interface in our structure is slightly different from that obtained at the surface of wafers dry oxidized at high temperatures.[27]

We emphasize that the observed decrease of the SPV for photon energies above the PVK band gap is related to a loss of carriers that can be separated by the electric field at the PVK/Si interface. This was illustrated here by decreasing the lifetime introduced in the modeling. However, a similar effect could be obtained by decreasing the PVK carrier mobility, as well as increasing the surface or interface nonradiative recombination velocity.

6. SUMMARY AND FUTURE OUTLOOK

In this paper, we have focused on PVK films deposited directly on crystalline Si substrates. PVK/Si direct heterojunction structures serve as a prospective combination for the fabrication of photovoltaic devices. They are simpler devices than conventional two-terminal PVK/Si tandem architectures, where the two materials are not in direct contact but are separated by tunnel or recombination layers,[9,15] and they are better suited to study energetics and band alignment between PVK and Si.

The successful design and fabrication of PVK/Si heterojunction devices require extensive characterization of the properties of the individual components and their interfaces by various complementary experimental methods and theoretical predictions. In this perspective, we have focused on the characterization of PVK/n-Si structures by the SPV method in its two operation modes: the SPV-MIS and the KPFM techniques providing complementary information about the optical absorption and photocarrier transport in the samples. Both methods have revealed a relatively large upward energy band bending in the silicon at the PVK/n-Si interface. It generates a positive SPV signal (SPV phase in the IVth quadrant) up to 2.07 eV. The combined analysis of the SPV-MIS amplitude and phase spectra and the KPFM transients recorded at illumination with 488 nm have evidenced a downward energy band bending at the PVK surface generating negative SPV (SPV phase in the IInd quadrant). The intense illumination causes the creation and movement of negative ions in the PVK, which accumulate at its surface. The SPV-MIS spectra suggest the existence of shallow defect levels at the PVK/n-Si interface, the density of which has increased after storage of the samples for one year in the dark in ambient conditions due to ageing effects. Nevertheless, the general spectral trend is preserved after one year, which confirms the major role of the silicon SCR in separating the carriers photogenerated in the structure.

Further use of the SPV technique in its different operation modes will be an effective means to provide complementary data about PVK/n-Si and PVK/p-Si heterostructures. In particular, information on carrier generation, transport, and recombination at different time scales can be obtained by this technique. In addition, the SPV-MIS amplitude spectra can deliver the PVK optical band gap and the presence of interface and bulk defect states, while the behavior of the energy band at the surface and interface can be found from the SPV-MIS phase spectra and the SPV sign in the KPFM measurements. All of these data can be complemented with information about the topography of the surface and interface potential obtained by KPFM.

Nevertheless, there are still open questions in the interpretation of the available SPV and KPFM experimental data, which need appropriate analysis. Here, we succeeded to interpret the shape of the SPS curves using drift−diffusion modeling. However, further modeling and simulation activities are needed to achieve a detailed quantitative assessment of the PVK/Si system and obtain a better understanding of the role of interface vs bulk properties. Comparing experimental and modeling results will deliver a unified picture of the information provided by the SPV technique in its different modes. Eventually, this will improve the diagnostic of PVK materials and the PVK/Si heterostructures and help in the optimization of such structures.

■ ASSOCIATED CONTENT

Supporting Information

The Supporting Information is available free of charge at https://pubs.acs.org/doi/10.1021/acsomega.2c07664.

Parameters used in the simulations of the SPV spectra and additional simulations considering carrier traps with energy positions closer to midgap of silicon (PDF)

■ AUTHOR INFORMATION

Corresponding Author

Vesselin Donchev − *Faculty of Physics, Sofia University, BG-1164 Sofia, Bulgaria;* orcid.org/0000-0003-3812-4474; Email: vtd@phys.uni-sofia.bg

Authors

Davide Regaldo − *Laboratoire de Génie Electrique et Electronique de Paris, Université Paris-Saclay, CentraleSupélec, CNRS, 91192 Gif-sur-Yvette, France;*

https://doi.org/10.1021/acsomega.2c07664
ACS Omega 2023, 8, 8125−8133

Laboratoire de Génie Electrique et Electronique de Paris, Sorbonne Université, CNRS, 75252 Paris, France; IPVF, Institut Photovoltaïque d'Ile-de-France, 91120 Palaiseau, France; orcid.org/0000-0002-6905-9479

Stefan Georgiev − *Faculty of Physics, Sofia University, BG-1164 Sofia, Bulgaria*

Aleksandra Bojar − *Laboratoire de Génie Electrique et Electronique de Paris, Université Paris-Saclay, CentraleSupélec, CNRS, 91192 Gif-sur-Yvette, France; Laboratoire de Génie Electrique et Electronique de Paris, Sorbonne Université, CNRS, 75252 Paris, France; IPVF, Institut Photovoltaïque d'Ile-de-France, 91120 Palaiseau, France*

Mattia da Lisca − *Laboratoire de Génie Electrique et Electronique de Paris, Université Paris-Saclay, CentraleSupélec, CNRS, 91192 Gif-sur-Yvette, France; Laboratoire de Génie Electrique et Electronique de Paris, Sorbonne Université, CNRS, 75252 Paris, France; IPVF, Institut Photovoltaïque d'Ile-de-France, 91120 Palaiseau, France*

Kiril Kirilov − *Faculty of Physics, Sofia University, BG-1164 Sofia, Bulgaria*

José Alvarez − *Laboratoire de Génie Electrique et Electronique de Paris, Université Paris-Saclay, CentraleSupélec, CNRS, 91192 Gif-sur-Yvette, France; Laboratoire de Génie Electrique et Electronique de Paris, Sorbonne Université, CNRS, 75252 Paris, France; IPVF, Institut Photovoltaïque d'Ile-de-France, 91120 Palaiseau, France*

Philip Schulz − *IPVF, Institut Photovoltaïque d'Ile-de-France, 91120 Palaiseau, France;* orcid.org/0000-0002-8177-0108

Jean-Paul Kleider − *Laboratoire de Génie Electrique et Electronique de Paris, Université Paris-Saclay, CentraleSupélec, CNRS, 91192 Gif-sur-Yvette, France; Laboratoire de Génie Electrique et Electronique de Paris, Sorbonne Université, CNRS, 75252 Paris, France; IPVF, Institut Photovoltaïque d'Ile-de-France, 91120 Palaiseau, France*

Complete contact information is available at: https://pubs.acs.org/10.1021/acsomega.2c07664

Notes

The authors declare no competing financial interest.

■ ACKNOWLEDGMENTS

This work was funded by and carried out in the framework of the PERMAVOLT project of the French-Bulgarian PHC RILA 2022 program (No. КП-06-Rila/10/16.12.2021 and No. 48059QL) for which funding is acknowledged. It was also supported by the European Regional Development Fund within the Operational Program "Science and Education for Smart Growth 2014−2020" under the Project CoE "National centre of mechatronics and clean technologies" BG05M2OP001-1.001-0008, as well as by the French government in the frame of the program of investments for the future (Programme d'investissement d'Avenir ANR-IEED-002-01).

■ REFERENCES

(1) Levine, I.; Vera, O. G.; Kulbak, M.; Ceratti, D. R.; Rehermann, C.; Márquez, J. A.; Levcenko, S.; Unold, T.; Hodes, G.; Balberg, I.; Cahen, D.; Dittrich, T. Deep Defect States in Wide-Band-Gap ABX3 Halide Perovskites. *ACS Energy Lett.* **2019**, *4*, 1150−1157.

(2) Zu, F.; Wolff, C. M.; Ralaiarisoa, M.; Amsalem, P.; Neher, D.; Koch, N. Unraveling the Electronic Properties of Lead Halide Perovskites with Surface Photovoltage in Photoemission Studies. *ACS Appl. Mater. Interfaces* **2019**, *11*, 21578−21583.

(3) Ma, J. Y.; Ding, J.; Yan, H. J.; Wang, D.; Hu, J. S. Temperature-Dependent Local Electrical Properties of Organic-Inorganic Halide Perovskites: In Situ KPFM and c-AFM Investigation. *ACS Appl. Mater. Interfaces* **2019**, *11*, 21627−21633.

(4) Dittrich, T.; Awino, C.; Prajongtat, P.; Rech, B.; Lux-Steiner, M. C. Temperature Dependence of the Band Gap of CH3NH3PbI3 Stabilized with PMMA: A Modulated Surface Photovoltage Study. *J. Phys. Chem. C* **2015**, *119*, 23968−23972.

(5) Futscher, M. H.; Deibel, C. Defect Spectroscopy in Halide Perovskites Is Dominated by Ionic Rather than Electronic Defects. *ACS Energy Lett.* **2022**, *7*, 140−144.

(6) Lee, J. W.; Kim, S. G.; Yang, J. M.; Yang, Y.; Park, N. G. Verification and Mitigation of Ion Migration in Perovskite Solar Cells. *APL Mater.* **2019**, *7*, No. 041111.

(7) Armaroli, G.; Ferlauto, L.; Lédée, F.; Lini, M.; Ciavatti, A.; Kovtun, A.; Borgatti, F.; Calabrese, G.; Milita, S.; Fraboni, B.; Cavalcoli, D. X-Ray-Induced Modification of the Photophysical Properties of MAPbBr3Single Crystals. *ACS Appl. Mater. Interfaces* **2021**, *13*, 58301−58308.

(8) Levine, I.; Hodes, G.; Snaith, H. J.; Nayak, P. K. How to Avoid Artifacts in Surface Photovoltage Measurements: A Case Study with Halide Perovskites. *J. Phys. Chem. Lett.*. American Chemical Society July 6, 2017, pp 2941−2943. DOI: 10.1021/acs.jpclett.7b01332.

(9) Elsmani, M. I.; Fatima, N.; Paul Jallorina, M. A.; Sepeai, S.; Sukor Su, M.; Ahmad Ludin, N.; Asri Mat Teridi, M.; Sopian, K.; Adib Ibrahim, M. Recent Issues and Configuration Factors in Perovskite-Silicon Tandem Solar Cells towards Large Scaling Production. *Nanomaterials* **2021**, *11*, 3186.

(10) Green, M. A.; Ho-Baillie, A.; Snaith, H. J. The Emergence of Perovskite Solar Cells. *Nat. Photonics* **2014**, *8*, 506−514.

(11) De Wolf, S.; Holovsky, J.; Moon, S. J.; Löper, P.; Niesen, B.; Ledinsky, M.; Haug, F. J.; Yum, J. H.; Ballif, C. Organometallic Halide Perovskites: Sharp Optical Absorption Edge and Its Relation to Photovoltaic Performance. *J. Phys. Chem. Lett.* **2014**, *5*, 1035−1039.

(12) Ul Kim, C.; Dae Jung, E.; Wook Noh, Y.; Kuk Seo, S.; Choi, Y.; Park, H.; Hoon Song, M.; Jin Choi, K.; Myoung Hoon Song, C. Strategy for Large-Scale Monolithic Perovskite/Silicon Tandem Solar Cell: A Review of Recent Progress. *EcoMat* **2021**, *3*, No. e12084.

(13) Lal, N. N.; Dkhissi, Y.; Li, W.; Hou, Q.; Cheng, Y. B.; Bach, U. Perovskite Tandem Solar Cells. *Adv. Energy Mater.* **2017**, *7*, No. 1602761.

(14) Köhnen, E.; Jošt, M.; Morales-Vilches, A. B.; Tockhorn, P.; Al-Ashouri, A.; Macco, B.; Kegelmann, L.; Korte, L.; Rech, B.; Schlatmann, R.; Stannowski, B.; Albrecht, S. Highly Efficient Monolithic Perovskite Silicon Tandem Solar Cells: Analyzing the Influence of Current Mismatch on Device Performance. *Sustainable Energy Fuels* **2019**, *3*, 1995−2005.

(15) Akhil, S.; Akash, S.; Pasha, A.; Kulkarni, B.; Jalalah, M.; Alsaiari, M.; Harraz, F. A.; Balakrishna, R. G. Review on Perovskite Silicon Tandem Solar Cells: Status and Prospects 2T, 3T and 4T for Real World Conditions. *Mater. Des.* **2021**, *211*, No. 110138.

(16) NREL. *Best Research-Cell Efficiency Chart*. https://www.nrel.gov/pv/cell-efficiency.html.

(17) Mariotti, S.; Turkestani, M.; Al; Hutter, O. S.; Papageorgiou, G.; Major, J. D.; Swallow, J.; Nayak, P. K.; Snaith, H. J.; Dhanak, V. R.; Durose, K. Direct Silicon Heterostructures with Methylammonium Lead Iodide Perovskite for Photovoltaic Applications. *IEEE J. Photovoltaics* **2020**, *10*, 945−951.

(18) Bojar, A.; Regaldo, D.; Alvarez, J.; Alamarguy, D.; Donchev, V.; et al. Surface Photovoltage Characterisation of Metal Halide Perovskite on Crystalline Silicon Using Kelvin Probe Force Microscopy and Metal-Insulator-Semiconductor Configuration. *EPJ Photovoltaics* **2022**, *13*, 18.

(19) Kronik, L.; Shapira, Y. Surface Photovoltage Phenomena: Theory, Experiment, and Applications. *Surf. Sci. Rep.* **1999**, *37*, 1−206.
(20) Melitz, W.; Shen, J.; Kummel, A. C.; Lee, S. Kelvin Probe Force Microscopy and Its Application. *Surf. Sci. Rep.* **2011**, *66*, 1−27.
(21) Donchev, V. Surface Photovoltage Spectroscopy of Semiconductor Materials for Optoelectronic Applications. *Mater. Res. Express* **2019**, *6*, No. 103001.
(22) Ivanov, T.; Donchev, V.; Germanova, K.; Kirilov, K. A Vector Model for Analysing the Surface Photovoltage Amplitude and Phase Spectra Applied to Complicated Nanostructures. *J. Phys. D: Appl. Phys.* **2009**, *42*, No. 135302.
(23) Walsh, A.; Stranks, S. D. Taking Control of Ion Transport in Halide Perovskite Solar Cells. *ACS Energy Lett.* **2018**, *3*, 1983−1990.
(24) Hoke, E. T.; Slotcavage, D. J.; Dohner, E. R.; Bowring, A. R.; Karunadasa, H. I.; McGehee, M. D. Reversible Photo-Induced Trap Formation in Mixed-Halide Hybrid Perovskites for Photovoltaics. *Chem. Sci.* **2015**, *6*, 613−617.
(25) Tennyson, E. M.; Roose, B.; Garrett, J. L.; Gong, C.; Munday, J. N.; Abate, A.; Leite, M. S. Cesium-Incorporated Triple Cation Perovskites Deliver Fully Reversible and Stable Nanoscale Voltage Response. *ACS Nano* **2019**, *13*, 1538−1546.
(26) Garrett, J. L.; Tennyson, E. M.; Hu, M.; Huang, J.; Munday, J. N.; Leite, M. S. Real-Time Nanoscale Open-Circuit Voltage Dynamics of Perovskite Solar Cells. *Nano Lett.* **2017**, *17*, 2554−2560.
(27) Poindexter, E. H.; Gerardi, G. J.; Rueckel, M. E.; Caplan, P. J.; Johnson, N. M.; Biegelsen, D. K. Electronic Traps and Pb Centers at the Si/SiO2 Interface: Band-Gap Energy Distribution. *J. Appl. Phys.* **1984**, *56*, 2844−2849.
(28) Herz, L. M. Charge-Carrier Mobilities in Metal Halide Perovskites: Fundamental Mechanisms and Limits. *ACS Energy Lett.* **2017**, *2*, 1539−1548.
(29) Caprioglio, P.; Stolterfoht, M.; Wolff, C. M.; Unold, T.; Rech, B.; Albrecht, S.; Neher, D. On the Relation between the Open-Circuit Voltage and Quasi-Fermi Level Splitting in Efficient Perovskite Solar Cells. *Adv. Energy Mater.* **2019**, *9*, No. 1901631.
(30) Stolterfoht, M.; Grischek, M.; Caprioglio, P.; Wolff, C. M.; Gutierrez-Partida, E.; Peña-Camargo, F.; Rothhardt, D.; Zhang, S.; Raoufi, M.; Wolansky, J.; Abdi-Jalebi, M.; Stranks, S. D.; Albrecht, S.; Kirchartz, T.; Neher, D. How To Quantify the Efficiency Potential of Neat Perovskite Films: Perovskite Semiconductors with an Implied Efficiency Exceeding 28%. *Adv. Mater.* **2020**, *32*, No. 2000080.

https://doi.org/10.1021/acsomega.2c07664
ACS Omega 2023, 8, 8125−8133